FORMATION OF MESO- AND MICRO-PORES IN FLY-ASH ZEOLITES USING A THREE-STEP ACTIVATION

BHAGWANJEE JHA and D. N. SINGH

about the authors

Bhagwanjee Jha
Dr. B.B.A. Government Polytechnic, Karad (DP)
Dadra and Nagar Haveli, India
E-mail: jha66b@yahoo.com

D. N. Singh
Indian Institute of Technology, Bombay, Powai,
Civil Engineering Department
Mumbai-400076, India
E-mail: dns@civil.iitb.ac.in

Abstract

Researchers have comprehensively characterized alkali-activated fly-ash (the residue) and ascertained its highly zeolitic nature. In order to evaluate its potential for application as an adsorbent for the decontamination of waste water, the decisive parameters have mostly been the cation-exchange capacity, the mineralogy and the morphology of the residue. However, a study of the pore characteristics (e.g., the size and volume) of such residues is still warranted to anticipate their contaminant transport and the diffusion phenomena as a type of geotechnical engineering material. In this situation, the present study demonstrates the evolution of pores in the fly-ash after alkali activation up to three steps, and simultaneously, its effects` on other characteristics (e.g., the specific gravity, specific surface area and the cation-exchange capacity) of three types of similarly synthesized residues (the first, produced by using a NaOH aqueous solution and the other two residues, the result of alkali activation using a NaOH spent solution, the filtrates). Based on N_2 gas absorption isotherms and infrared transmittance spectra, residues obtained from the second and third steps, each involving 24 hours of treatment using filtrates of 1.5-M NaOH, are established to be significantly enriched in the finer meso- and micro-pores, respectively, in comparison with a pure and macro-porous zeolite 4A.

keywords

fly-ash, hydrothermal treatment, three-step activation, pore characteristics

ABBREVIATIONS

AFA	alkali-activated fly-ash
BET	Brunauer-Emmett-Teller
EGME	ethyle glycol monoethyl ether
FAF	fly-ash filtrate
FAR	filtrate-activated residues
FEG-SEM	field-emission gun scanning electron microscopy
FT-IR	Fourier-transforms infrared
JCPDS	Joint Committee on Powder Diffraction Standards
MPA	micro-pore area
MPV	micro-pore volume
RZP	reference zeolite 4A powder
XRF	X-ray fluorescence
XRD	X-ray diffraction

NOMENCLATURES

CEC	cation-exchange capacity
G	specific gravity
M	molarity of NaOH
SSA	specific surface area
SSA_{BET}	surface area by BET method
SSA_{EGME}	surface area by EGME method

1 INTRODUCTION

Alkali-activated fly-ash (AFA) is now an established synthetic material, as an adsorbent, for many industrial applications, e.g., waste-water and flue-gas treatment [1-6]. The credit goes to the cation-exchange capacity of the AFA, which has been thoroughly explored in the past for its likely use as a constituent for polycrystalline zeolites (the geotechnical composites) [1-8].
More specifically, the degree of coordination between $[SiO_4]^{4-}$ and $[AlO_4]^{5-}$ tetrahedra, present in such zeolites, governs the type of 3D framework and the creation of network of pores (e.g., voids and open spaces), which in turn affect the geotechnical application of such zeolites for waste-water or flue-gas decontamination (an

environmental cleanup project) [8]. In fact, the evolution of pores in the AFA, in general, and the presence of a distinct pore size and pore volume may be helpful in deciding their suitability for adsorbing the corresponding size of a heavy-metal contaminant (the cation) [5,8,11]. Accordingly, in the past BET analyses have been useful to quantify the pore size and the overall porosity of the AFA [8-10,12-15]. However, state-of-the-art information is limited to the zeolitic characteristics of the AFA obtained from the fly-ash–NaOH interaction by employing various hydrothermal techniques in: (1) a single step [1-7,10,11,13,16,], (2) two steps [17], and (3) three steps [18]. However, proper attention has not been given to a detailed investigation of the pore characteristics of the AFA, which is supposed to be of prime importance for the cation diffusion centric geotechnical application of such material [9]. Based on past reports on common fly-ash zeolites (e.g., Na-P1, hydroxysodalite, analcime, Na-A, Na-X and Na-Y etc.), facts about their pores have mostly been borrowed from standard data files of JCPDS (1994) [11,16], which deals with the pure form of these zeolites. To decide about the conformity of the ash zeolites to its pure zeolite counterpart, it still remains a challenging task to investigate the actual pore characteristics of the AFA, which can, in turn, be suitably evaluated for its contaminant diffusion and/or transport phenomenon, as a geotechnical engineering material [2-9,15,16]. In such a situation, the present study demonstrates how a three-step hydrothermal treatment of a fly-ash with NaOH or fly-ash filtrate (FAF) results in a remarkable growth of the pore sizes in the AFA. As such, the manuscript is framed to showcase these improvements in the AFA in detail. Also, attempts have been made to correlate the Brunauer-Emmett-Teller (BET) isotherms type with the specific gravity (***G***), the specific surface area (***SSA***), the cation exchange capacity (***CEC***), the Fourier transform infrared (FT-IR) transmittance bands, the X-ray fluorescence (XRF), the X-ray diffraction (XRD) studies and the field-emission-gun scanning electron microscopy (FEG-SEM) of the residues.

2 EXPERIMENTAL DETAILS

The original fly-ash (OFA) was procured from the hopper of an electrostatic precipitator of a thermal power plant in Maharashtra, India. The NaOH used for preparing its stock solution (molarity = 1.5-***M***) in deionized water was supplied by Thomas Baker, Mumbai, India. In order to activate the OFA and synthesize pure fly-ash zeolites, the liquid-to-solid ratio, i.e., a NaOH/OFA equal to 10, was maintained for preparing the fly-ash–NaOH slurry [7]. To investigate the residue-filtrate interaction (i.e., ignored by previous researchers favoring a conventional hydrothermal treatment of the fly-ash–NaOH slurry only), the present manuscript addresses the hydrothermal treatment of the fly-ash up to three successive steps, in line with Jha and Singh (2013) [18], each of 24 hours at 100 °C. In particular, Step-2 and Step-3 were carried out by treating a mixture of the residue, AFA, and the filtrate, FAF of the previous step by maintaining the liquid-to-solid ratio, FAF/AFA equal to 10, in each case throughout the experiments. To evaluate the effect of these steps, each residue was characterized for physico-chemico-mineralogical, morphological and Fourier-transform infrared (FT-IR) characteristics [7-11,19,20]. For the sake of simplicity, the residue was designated by combining three parameters in a sequence: (i) a value of the molarity (***M***) of NaOH for the stock solution used in Step-1, and (ii) a designation for the step of the treatment and (iii) the time allowed in each step. For example, the designations 1.5-S1-24, 1.5-S2-24 and 1.5-S3-24 correspond to the residues obtained after the treatments by using 1.5-***M*** NaOH in Step-1, Step-2 and Step-3, respectively, each for 24 hours. To ascertain the proximity of the residue to the pure zeolite, Na-A (i.e., zeolite 4A) was used as a reference zeolite powder (RZP) material for the comparative study.

3 CHARACTERIZATION

The specific gravity, ***G***, of the sample was determined by employing an Ultra Pycnometer (Quanta chrome, USA), which works on the principle of the adsorption of helium gas [7]. The results of this analysis are presented in Table 1.

Table 1. Important parameters of fly-ash, activated fly-ashes and zeolite RZP.

Parameter	OFA	1.5-S1-24	1.5-S2-24	1.5-S3-24	RZP
G	2.18	2.94	2.63	2.55	2.14
SSA_{BET} (m^2/g)	2.83	7.04	7.38	6.23	1.87
SSA_{EGME} (m^2/g)	7.0	33.9	110.5	155.6	94.5
CEC (meq/100g)	8	296	470	843	450

The Na^+ cation exchange capacity (***CEC***) of the residue was determined by following the ammonium acetate method [7,11]. The result for ***CEC*** is listed in Table 1. The investigations were carried out to study the micro-pore area (MPA) and the micro-pore volume (MPV) present in these samples. A BET set up (ASAP 2020 system V 3.01 H fitted with Micromeritics patented isothermal

jackets, Norcross, GA 30093-1877) was used and a set of standard procedures was followed for this purpose [12-15,18]. The analysis temperature was maintained at that of liquid N_2 (i.e., 195.489 °C). Also, the sample (maximum 1g) was degassed automatically under vacuum (5×10^{-3} mmHg) [19]. The results, e.g., the ***SSA***, the pore volume and types of pore sizes e.g., micro-pores below 2 nm, meso-pores between 2 and 50 nm and macro-pores above 50 nm, are presented in Tables 1 to 2 and Figs. 1 to 2. The surface area, ***SSA***, of the samples was also calculated by resorting to the ethyl-glycol-monoethyl ether (EGME) adsorption method [11] and the results of this analysis are presented in Table 1. Furthermore, a Fourier transform infrared (FT-IR) set up [17-19] was employed to generate the transmittance spectra of these samples by following procedures suggested by Jha and Singh (2011) [9]. The FT-IR spectra are presented in Fig. 3. The chemical compositions of the residues were investigated by carrying out quantitative analyses with the help of an XRF set up (Philips 1410, The Netherlands) [7]. The results of this analysis are presented in Table 2. Furthermore, the fly-ash and the residues were subjected to a field-emission-gun scanning electron microscopy (FEG-SEM) set up (JEOL JSM-7600F, Japan) to reveal their morphological details (e.g., surface pores and the shape and size of the crystals) [6,12,14,15]. The results of this analysis are presented in Fig. 4. Also, the mineralogy of the residue was investigated with the help of an X-ray diffraction spectrometer set up (Philips, Eindhoven, The Netherlands) and the results, as depicted in Fig. 5, were analyzed by using the JCPDS data files (1994) [20].

4 RESULTS AND DISCUSSION

In agreement with previous researchers' findings (Kolay and Singh, 2002) this study ascertains an increase in the specific gravity (***G***) and the specific surface area (***SSA***) from the fly-ash OFA to the residue 1.5-S1-24 obtained from the Step-1 treatment, as is clear from Table 1. It is also clear in this table that Step-2 results in filtrate activated residues (FARs), which reduced the ***G*** and increased the ***SSA*** values, compared to the residues of Step-1. These changes in the FAR can be attributed to a significantly increased pore volume, from 0.01725 to 0.036 cm^3/g (by 108%), as observed in Table 2. Incidentally, the Step-2 treatment is also effective in (i) the creation of smaller meso-pores (3 to 10 nm) by 6.94% (ii) a reduction in larger meso-pores, i.e.,10 to 50 nm by 5.56%, and (iii) a reduction in macro-pores by 1.4%. Accordingly, such an improvement in the pores in the Step-2 residue FAR can be responsible for the remarkably enhanced cation-exchange capacity (***CEC***) (refer to Table 1). This can be equally attributed to increased ***SSA*** values, in general; however, the ***SSA*** values obtained from the BET (N_2 gas relative pressure in between 0.05 and 0.3) correspond to the external pores, while that computed by the EGME adsorption corresponds to the total of the external and internal pores in the residues. Accordingly, Step-2 is believed to form more internal pores. Furthermore, from Table 3, quantities of SiO_2 and Al_2O_3 are found to increase due to the Step-2 treatment. This reveals that the silica dissolved during Step-1 in the filtrate is regained during the Step-2 treatment and in turn there could be (i) an improved coordination between the Si and Al tetrahedra and hence (ii) a better pore size distribution in the residue, as is apparent from Table 2.

Furthermore, it is interesting to note the characteristic changes in the residues obtained from Step-3, which results in an exceptionally high $\boldsymbol{SSA}_{\mathrm{EGME}}$ value (refer Table 1). This is indicative of the formation of finer meso-pores (2–3 nm by 4.25% by volume). Most encouraging is that this step also creates some mico-pore volume by 2.1%, which can be attributed to the extraordinarily high ***CEC*** up to 843 meq/100g (i.e., higher than that of the reference zeolite RZP) of the residues 1.5-S3-24. In fact, the reason behind the relatively low ***CEC*** of the RZP could be its smaller surface area ***SSA***, corresponding to macro-pores, as highlighted in Table 2. Furthermore, from Fig. 1 it is clear that the zeolite 4A exhibits more N_2 gas condensation at higher pressures than the fly-ash.

Table 2. Pore size distribution for fly-ash, activated fly-ashes based on a BET analysis.

Sample	Total Pore volume (cm^3/g)	Pore volume (%) contribution of various sizes (nm)				
		< 2	2 to 3.0	3.0 to 10	10 to 50	> 50
		Micro	Meso			Macro
OFA	0.00195	0	0	0	35.89	64.10
1.5-S1-24	0.01725	-	-	-	33.33	66.67
1.5-S2-24	0.036	-		6.94	27.77	65.27
1.5-S3-24	0.0235	2.1	4.25	2.12	25.53	66.00
RZP	0.00325	-	-	-	-	100.00

Note: the dash indicates that the measurement is below the detection limit

Both these isotherms reveal fewer interconnected micro-pores, as is clear from the gap between the absorption and desorption isotherms and their open ends. Also, out of the three isotherms and the type-III hysteresis [12] for alkali-activated residues (the treated fly-ashes), 1.5-S2-24 undergo a remarkably high gas condensation in the capillaries between the meso-pores, which also exhibit a hysteresis lag between the two curves (absorption and desorption), commonly blamed for the pore blocking during desorption (referred to as the ink-bottle effect) in the residues. Such effects are relatively less noticeable in isotherms of residues 1.5-S3-24, which might be a revelation of well-interconnected micro- to meso-pores. More precisely, the dominant pore diameter in these samples was shown as black and red arrows on the dV/[dlog(D)] verses pore diameter (D) curves corresponding to both adsorption and desorption, respectively, depicted in Fig. 2.

From this figure it is clear that the desorption curves terminate at smaller pore diameters than the adsorption curves. This can be attributed to (i) the reduced pore openings, which is an indication of gas condensation on the boundaries of the initial pores, (ii) the larger pores, i.e., the meso-pores get blocked and hence a reduced dominant pore diameter from the desorption trends. Such a pore-blocking effect is found to be very serious in the case of zeolite 4A, in which the desorption curve shifts remarkably to smaller pores. Exceptionally, only micro-pores are observable in the residue 1.5-S3-24, in which negligible pore blocking is possible for a pore diameter of less than 100 Å.

Slightly similar pore characteristics for these residues are observed from the FT-IR spectra, as indicated in Fig. 3.

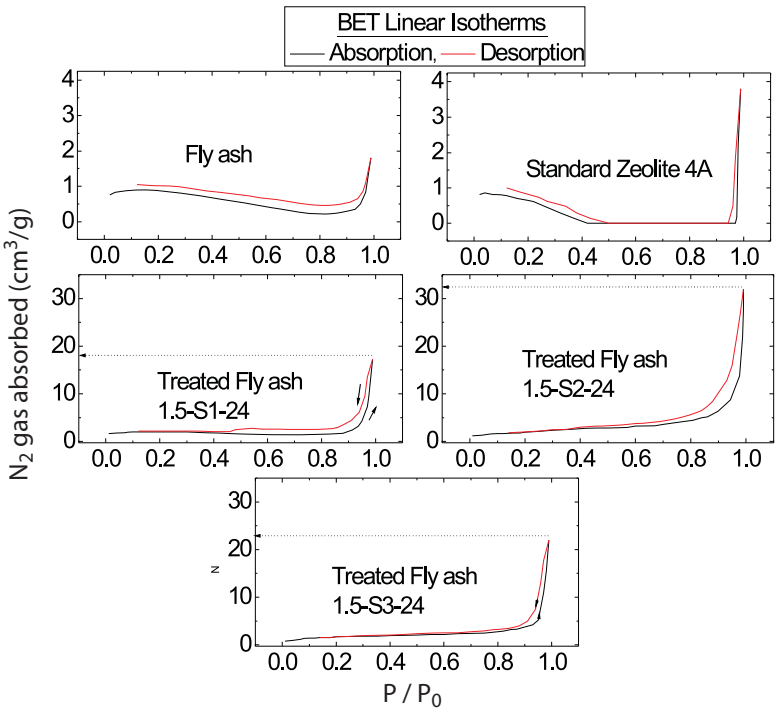

Figure 1. Variation in N_2 gas absorption with the P/P_0 ratio maintained in the BET analysis.

Table 3. Chemical composition of fly-ash, activated fly-ash residues and the zeolite RZP.

Samples	Oxides (by Wt. %)											
	Al_2O_3	BaO	CaO	Fe_2O_3	K_2O	MgO	MnO_2	Na_2O	P_2O_5	SiO_2	SrO	TiO_2
OFA	26.05	0.14	1.88	5.14	0.66	0.39	0.16	0.054	10.5	63.85	0.25	1.52
1.5-S1-24	25.57	0.10	1.63	5.51	0.38	0.34	0.05	10.60	NA	48.71	0.04	1.51
1.5-S2-24	26.47	0.09	1.85	5.53	0.27	0.41	0.05	9.77	0.04	53.95	0.04	1.51
1.5-S3-24	34.55	0.09	1.86	3.60	0.30	0.39	0.05	8.57	0.05	49.13	0.04	1.40
RZP	46.04	0.03	0.22	0	0	0	0.02	16.87	0.02	36.57	0.01	0.24

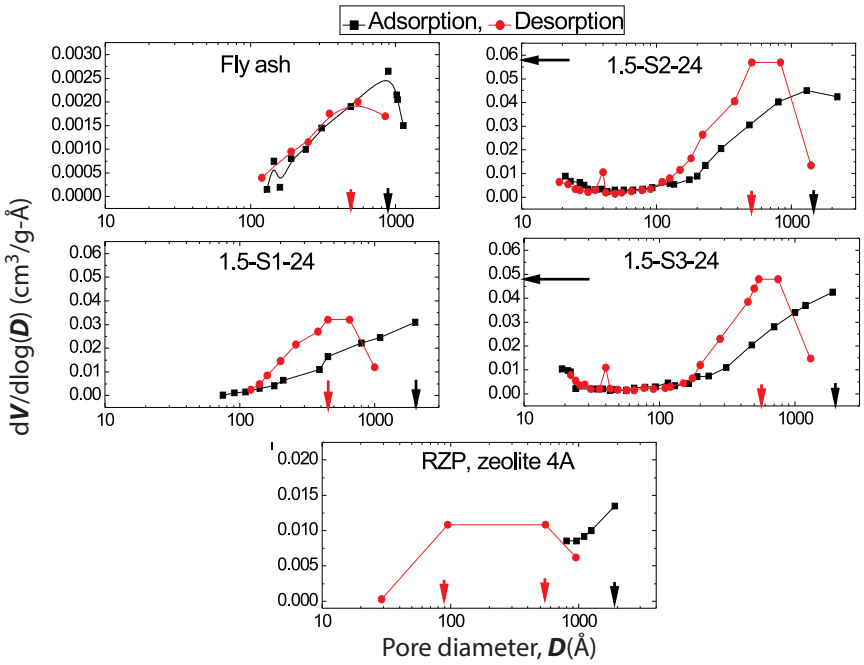

Figure 2. BJH sorption curves for the fly-ash, activated fly-ash residues and zeolite, where the black and red arrows represent the dominant pore diameters corresponding to N_2 gas adsorption and desorption, respectively.

From this figure the spectrum of zeolite 4A (designated as RZP) shows sharper bands than the residues 1.5-S2-24, which competes in the transmittance values up to nearly half of its counterpart at wave numbers, e.g., 3455, 1656, and 999 cm^{-1}. Based on the very sharp bands at 563 cm^{-1}, it is thought that the zeolite 4A is made up of a relatively more polymerized double-ring framework than the residues 1.5-S2-24 [20]. In contrast, the pore openings represented by the bands at 448 cm^{-1} are similar for the residues 1.5-S2-24 and the zeolite RZP [7,17,18,20]. Surprisingly, the zeolite RZP and the residues 1.5-S3-24 display a negligible band at 1456 cm^{-1} (i.e., indicative of carbon or nitrogen to oxygen bonds), which might be beneficial for the residues to have a high ***CEC*** (refer Table 1). In addition, the sharper band in the spectrum of the residue 1.5-S3-24 at 448 cm^{-1} (i.e., an indication of micro-pores) is in agreement with the BET results, as is clear from Table 2).

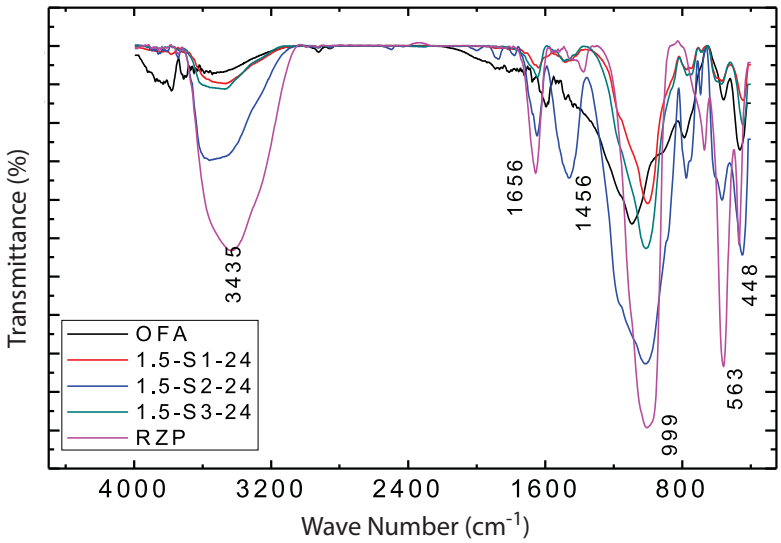

Figure 3. FT-IR spectra of the fly-ash OFA, its residues 1.5-S1-24, 1.5-S2-24, 1.5-S3-24 and the zeolite 4A.

To clarify the surface pores in these samples, Fig. 4 depicts the morphological transitions in these samples. As compared to the fly-ash OFA (i.e., a matrix of larger particles of quartz, mullite, small spherules of glass and cenospheres), the residue 1.5-S3-24 (i.e., agglomerates of spherules and cubic-to-cuboidal shaped crystals, conforming to those in the micrographs of zeolite RZP) exhibits significant changes in the particle morphology and pores (the opening between the crystals and also within their framework). A similarity between the zeolite RZP and the residues 1.5-S3-24 is also established from their XRD diffractograms, depicted in Fig. 5, which exhibits many new mineral peaks conforming to zeolite 4A, Na-P1 and X [20].

Incidentally, inactive minerals (e.g., quartz and mullite) present in the OFA are converted to zeolite Na-P1 after Step-1, which later exhibits higher intensity counts corresponding to Step- 2, and further upgraded to zeolite 4A, after the Step-3 activation. Accordingly, the increased intensity counts of zeolite Na-P1 and growth of zeolite 4A, present in 1.5-S3-24, are indicative of their atomic-level packing and transition in pore characteristics, as well [15,20]. Thus, based on all the above discussions, the residues 1.5-S3-24 can be graded as a superior material, which is significantly enriched in ***CEC***, highly porous and hydroxylated and hence a better material for waste-water decontamination.

5 CONCLUSIONS

The alkali-activated fly-ash obtained from Steps-2 and 3 became gradually enriched in smaller sizes of meso-pores (2 to 10 nm). Such pores are partially changed to micro-pores in the fly-ash residues 1.5-S3-24 obtained from Step-3 treatment using 1.5-***M*** NaOH and an activation time of 24 hours. Also, a significant increase in the specific surface area, pore volume and the formation of the zeolites 4A and Na-P1 are responsible for a high cation-exchange capacity of this residue. These improvements in the residues of Steps-2 and 3 are in line with the major bands in their FT-IR spectra and FEG-SEM micrographs.

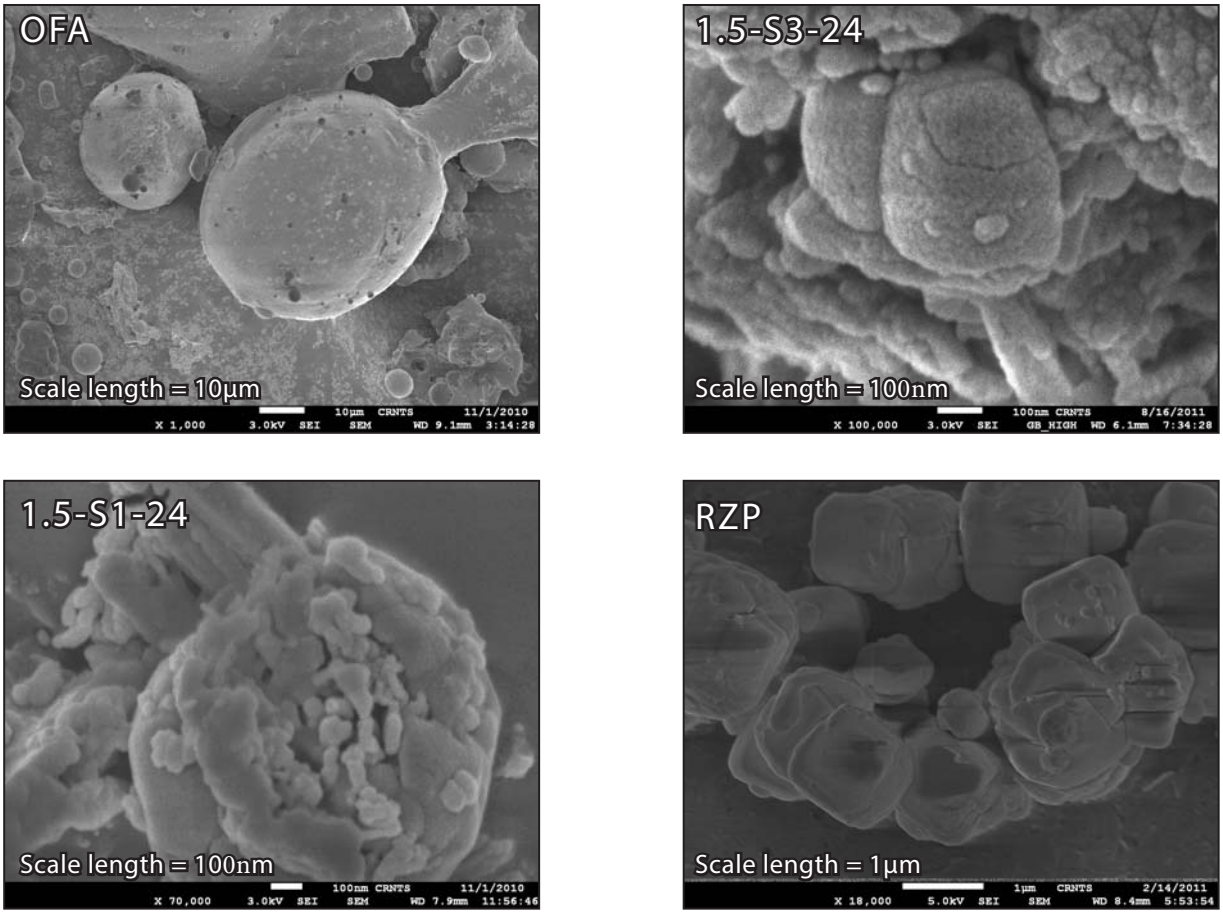

Figure 4. FEG-SEM micrographs of the fly-ash OFA, its conventional residue 1.5-S1-24, most porous residues 1.5-S3-24 and the RZP zeolite 4A.

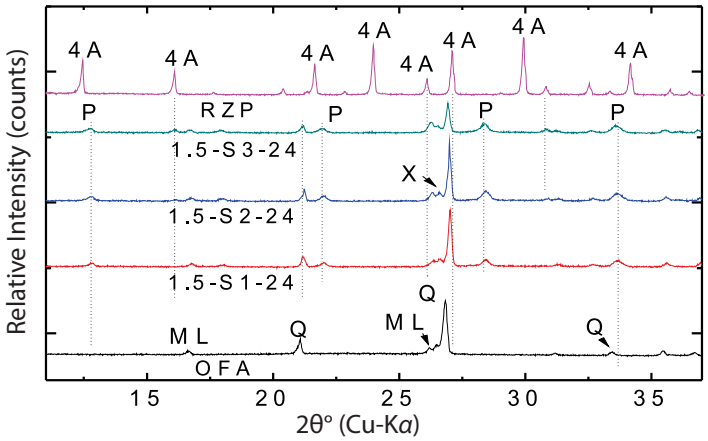

Figure 5. XRD diffractogram of the fly-ash OFA, its residues 1.5-S1-24, 1.5-S2-24, 1.5-S3-24 and zeolite 4A, where 4A, P, X, ML and Q designate zeolites 4A, Na-P1, Na-X, mullite and quartz, respectively.

REFERENCES

[1] Lin, C.F., His, H.C. (1995). Resource recovery of waste fly-ash: synthesis of zeolite-like materials. *Environ. Sci. Technol.*, Vol. 29, pp. 1109-1117.

[2] Berkgaut, V., Singer, A. (1996). High capacity cation exchanger by hydrothermal zeolitization of coal fly-ash. *Appl. Clay Sci.*, Vol. 10, pp. 369-378.

[3] Kim, W., Seung-Hoon, Ahn, B.J. (1997). Synthesis of Na-P1 zeolite from coal fly-ash, *J. Ind. Eng. Chem.*, Vol. 3(3), pp. 185-190.

[4] Kolay, P.K., Singh, D.N., Murti, M.V.R. (2001). Synthesis of zeolites from lagoon ash. *Fuel*, Vol. 80(5), pp. 739-745.

[5] Querol, X., Moreno, N., Umana, J.C., Alastuey, A., Hemandez, E., Lopez-Soler, A., Plana, F. (2002). Synthesis of zeolites from coal fly-ash: an overview. *Int. J. Coal Geol.*, Vol. 50, pp. 413-423.

[6] Medina, A., Gamero, P., Almanza, J.M., Vargas, A., Montoya, A., Vargas, G., Izquierdo, M. (2010). Fly-ash from a Mexican mineral coal. II. Source of W zeolite and its effectiveness in arsenic (V) adsorption. *J. Hazard. Mater.*, Vol. 181, pp. 91-104.

[7] Jha, B., Singh, D.N. (2012). Zeolitization characteristics of fly-ashes from wet- and dry-disposal systems. *Acta Geotech. Slov.*, Vol. 9(2), pp. 63-71.

[8] Tyrologou, P., Dudeney, A.W.L., Grattoni, C.A. (2005). Evolution of porosity in geotechnical composites. *Magn. Reson. Imaging*, Vol. 23, pp. 765-768.

[9] Shekelford, C. (2013). The role of diffusion in environmental geotechnics. Poceedings of the 18th International Conference on Soil Mechanics and Geotechnical Engineering, Paris.

[10] Franus, W. (2012). Characterization of X type zeolite prepared from coal fly-ash. Pol. Environ. Stud., Vol. 21(2), pp. 337-343.

[11] Jha, B., Singh, D.N. (2011). A review on synthesis, characterization and industrial application of fly-ash zeolites, *J. Mater. Educ.*, Vol. 33(1-2), pp. 65-132.

[12] Gregg, S.J., Sing, K.S.W. (1982). Adsorption, surface area and porosity. Academic Press Inc, 2nd ed., London.

[13] Ojha, K., Pradhan, N.C., Samanta, A.N. (2004). Zeolite from fly-ash synthesis and characterization. *Bull. Mater. Sci.*, Vol. 27, pp. 555-564.

[14] ASAP 2020. Accelerated surface area and porosimetry system. Operator's Manual V3.0, Micromeritics Instrument Corporation, 2004-2006.

[15] Neimark, A.V., Sing, K.S.W., Thommes, M. (2008) Surface area and porosity, Handbook of Heterogeneous Catalysis, Wiley.

[16] Singh, D.N., Kolay, P.K. (2002). Simulation of ash water interaction and its influence on ash characteristics. *Prog. Energy Combus. Sci.*, Vol. 28 (3), pp. 267-299.

[17] Jha, B., Nevin, K., Singh, D.N. (2014). Establishing two-stage interaction between fly-ash and NaOH by X-ray and infrared analyses, *Front. Environ. Sci. Eng.*, doi: 10.1007/s11783-014-0630-8.

[18] Jha, B., Singh, D.N. (2013). A three step process for purification of fly-ash zeolites by hydrothermal treatment, *Appl. Clay Sci.*, http://dx.doi.org/10.1016/j.clay.2013.12.035.

[19] Santen, R.A.V., Man, A.J.M.D., Kramer, G.J. (1992). Chemical bonding in zeolites, Zeolite Microporous Solids: Synthesis, Structure, and Reactivity, Kluwer Academic Publishers, Netherlands.

[20] Joint committee on powder diffraction standards. (1994), Philadelphia-19103.